



Science Arts & Métiers (SAM)

is an open access repository that collects the work of Arts et Métiers Institute of Technology researchers and makes it freely available over the web where possible.

This is an author-deposited version published in: <https://sam.ensam.eu>
Handle ID: [.http://hdl.handle.net/10985/10916](http://hdl.handle.net/10985/10916)

To cite this version :

Elodie ARLAUD, Sofia COSTA D'AGUIAR, Etienne BALMES - Validation of a reduced model of railway track allowing long 3D dynamic calculation of train-track interaction - In: IACMAG, Japon, 2014-09 - IACMAG - 2014

Any correspondence concerning this service should be sent to the repository

Administrator : scienceouverte@ensam.eu



Validation of a reduced model of railway track allowing long 3D dynamic calculation of train-track interaction.

E. Arlaud

SNCF Innovation et Recherche, Paris, France

Arts et Métiers ParisTech, Laboratoire PIMM, CNRS UMR 8006, Paris, France

S. Costa D'Aguiar

SNCF Innovation et Recherche, Paris, France

E. Balmes

Arts et Métiers ParisTech, Laboratoire PIMM, CNRS UMR 8006, Paris, France

ABSTRACT: In order to face challenges of increased traffic and speed on their infrastructures, railway companies need to develop numerical tools able to predict the dynamic behaviour of the track. Currently, two approaches are widely used: the first one is a train-based methodology in which train dynamic is well reproduced but track is only represented as equivalent springs, the second one is a FEM model or FEM/BEM model of track in which the train is simply modeled as a moving load but the complexity of track taken into account. Dynavoie software studied in this work aims to offer a new approach by representing in details both track and train. Understanding train-track interaction requires transients on long track segments, leading to very large finite element models and high computation time. The specificity of Dynavoie software is to use periodic properties of the track to generate a reduced slice model, and then build the track as a combination of these slices. Computation time is then highly reduced. The present work focuses on the initial step of the model reduction where computations in the frequency and wave domains are used. The resulting 3D periodic computations are compared to 2.5D FEM/BEM results from the literature and the content of the receptance curve is discussed in relation with dispersion curves.

1 INTRODUCTION

Nowadays, trends in railways are for more traffic at higher speeds (Krylov 1995). This statement leads to an increase of track mechanical loads, which implies more maintenance work. However, maintenance work is costly and performed at night when there are no operating trains, which leads to big challenges both in management and in the ability to do the whole work in the imparted time at a reasonable cost (Esveld 1997). In order to face this challenge, railway companies are willing to improve their current tracks design in order to increase the life span of their infrastructures, notably by introducing under sleeper pads, ballast mats, or improving bearing soil capability (Esveld 1997).

Numerical models of tracks could then be a tool to help railway companies to specify the best solution for a given site (Esveld 2001), to check if these designs are really a progress regarding the whole track structure and to predict the behaviour of a given section of track, complementing *in-situ* mea-

surements. Several numerical models have been proposed to represent track behaviour. As Finite Element Models (FEM) are widely used for engineering purposes, various authors (Hall 2003, Araújo 2010, Kouroussis et al. 2011, Banimahd and Woodward 2007, Connolly et al. 2014, among others), have proposed an approach based on 3D FEM to model railway tracks. The main drawbacks of these models are the large computational time, the large storage capabilities required, the finite soil layer and wave reflections at boundaries. To reduce time computation, authors (Ribeiro 2012, Fernandes et al. 2014) have proposed 2D with modified plane strain FEM models, which allows good description of the track geometry but implies approximation regarding cross section of track. Even if the model is two dimensional, a track width can be specified to compute stress in layers. This methodology leads to approximations since the repartition of stress is not uniform in the width of the track. Moreover, a 3D computation has to be made in parallel to determine this value. Accounting for

track periodicity on its developing direction, some authors have proposed a coupled FEM-BEM numerical model in 2.5 D, which implies approximations on the track geometry (Yang et al. 2003, François et al. 2010, Alves Costa et al. 2012, among others) or in 3D representing the whole problem in one generic cell (Chebli et al. 2008). Time computation is then reduced but calculations can only be made in the frequency domain, implying uniformity of track in its developing direction.

Dynavoie is a finite element model that fully takes into account interactions between track, considering all its components, and train. This numerical model, used and described hereafter, presents an hybrid approach between 2.5D FEM calculation and 3D FEM. It is based on the finite element representation of a "slice" (basic cell with one sleeper repeated to form the track) of the track and uses track periodicity to reduce the number of degrees of freedom to take into account. This methodology allows both a good reproduction of track geometry and low time computation.

The aim of this work is to assess the model ability to represent track behaviour at the frequencies of interest, that is to say at least between 0 and 100 Hz.

A comparison with a 2.5 D FEM/BEM model is undertaken in order to verify the accuracy of the methodology employed. Then, the results are used to explicit the content of the track receptance curve, notably the resonance peaks and their links with eigen modes.

2 3D CALCULATION OF THE FREQUENCY RESPONSE OF TRACK

The methodology employed hereafter to exploit periodicity of track is derived from the work of Sternchüss (2009) on bladed disks, and is similar to that of Chebli et al. (2008) for railway tracks.

2.1 Direct and inverse Fourier transforms in the spatial domain

A structure is said spatially periodic when it is composed of cells geometrically identical, generated by a translation on a predefined direction from the reference cell. The reference cell width is Δx .

The fields studied in the model can then be discretized using this periodicity, that is to say each function u can be defined by values $u_n = u(x_n)$ where x_n is a set of values of x , n being in $[-\infty \infty]$. Then, for all n , $x_n = n\Delta x$ and $u_n = u(n\Delta x)$.

One can then compute Fourier transform

$$U(\kappa_{cx}) = \sum_{n=-\infty}^{\infty} u(n\Delta x) e^{-i\kappa_{cx}n} \quad (1)$$

where $U(\kappa_{cx})$ is a complex shape defined on the mesh composed of repeated cells.

The conventions used in this work regarding Fourier transform are the following:

- n_{cx} is the wavelength or spatial periodicity in number of cells, so $n_{cx} \in [1 \infty]$. The physical wavelength λ_x in length unit is then given by $\lambda_x = n_{cx} \times \Delta x$
- The discrete wavenumber κ_{cx} in rad/number of cells is then given by $\kappa_{cx} = 2\pi/n_{cx}$, so $\kappa_{cx} \in [0 2\pi]$, and the physical wavenumber k_x in rad/unit of length by $k_x = 2\pi/\lambda_x$. The relationship between both is $k_x = \kappa_{cx}/\Delta x$.

The inverse Fourier transform allows to recover physical field u based on its Fourier transform U

$$u(n\Delta x) = \frac{1}{2\pi} \int_0^{2\pi} U(\kappa_{cx}) e^{i\kappa_{cx}n} d\kappa_{cx} \quad (2)$$

For a fixed value of the wavenumber κ_{cx} , the field u is simply equal to

$$u(n\Delta x) = \text{Re}(U(\kappa_{cx}) e^{i\kappa_{cx}n}) \quad (3)$$

This property allows recovering values in the whole space, knowing only those taken on the first cell.

Looking at equation 1, U is real if κ_{cx} is equal to 0, π or 2π .

As for all $n \in [0 \infty]$, $\cos(n\kappa_{cx}) = \cos(n(2\pi - \kappa_{cx}))$ and $\sin(n\kappa_{cx}) = -\sin(n(2\pi - \kappa_{cx}))$, $U_{\kappa_{cx}}$ and $U_{2\pi-\kappa_{cx}}$ are conjugate.

Taking into account this last property, and knowing the Fourier transform U , the real-valued field u is recovered computing the inverse Fourier transform given by

$$u(n\Delta x) = \frac{1}{2\pi} \int_0^{\pi} 2(\text{Re}(U(\kappa_{cx})) \cos(n\kappa_{cx}) - \text{Im}(U(\kappa_{cx})) \sin(n\kappa_{cx})) d\kappa_{cx} \quad (4)$$

As κ_{cx} can take any value in $[0 2\pi]$ which is a continuous interval, numerical applications must make a choice regarding which values of κ_{cx} to consider and how to build the numerical approximation of the inverse transform. Since the integral is a linear function, one can express its result as a linear operator

$$\{u(n\Delta x)\} = [E_{nk}] \begin{Bmatrix} \text{Re}(U(\kappa_{cx})) \\ \text{Im}(U(\kappa_{cx})) \end{Bmatrix} \quad (5)$$

The size of matrix $[E]$ is then $n \times 2k$, with n corresponding of the number of slices that the user wants to represent and $k \in [1 N]$ the number of wavenumbers chosen, with the convention $\kappa_0 = 0$ and $\kappa_{N+1} = \pi$. This matrix is defined as following:

$$E_{n(2k-1)} = \cos(n\kappa_k) \frac{[(\kappa_{k+1} - \kappa_k) + (\kappa_k - \kappa_{k-1})]}{2\pi}$$

$$E_{n(2k)} = -\sin(n\kappa_k) \frac{[(\kappa_{k+1} - \kappa_k) + (\kappa_k - \kappa_{k-1})]}{2\pi} \quad (6)$$

which corresponds to a simple integration rule assuming $U(\kappa_{cx})$ constant over the interval $[(\kappa_k + \kappa_{k-1})/2, (\kappa_{k+1} + \kappa_k)/2]$.

2.2 Continuity condition

The properties mentioned above are applied to the displacement $\{q\}$ defined on the degrees of freedom (DOF) of the structure.

Since motion between adjacent cells is continuous a condition must be introduced. The response on a left cell edge has to be equal to that of the preceding cell right edge, thus $\{q_{left}(n\Delta x)\} = \{q_{right}((n-1)\Delta x)\}$. As each q_n represents all the displacements at the DOF of the cell n , one can define the observation matrices $[c_l]$ and $[c_r]$ (the same for all cells if the domain is regularly meshed), which for each cell allow to extract on the whole DOFs the ones corresponding to respectively left and right boundaries.

For a response at a given wavenumber, taking to account the equation 3, the condition can be written as $[c_l] \{Q(\kappa_{cx})\} = [c_l] \{Q(\kappa_{cx})\} e^{-2i\kappa_{cx}}$ which, differentiating real and imaginary parts, leads to

$$[C(\kappa_{cx})] \begin{Bmatrix} \text{Re}(Q(\kappa_{cx})) \\ \text{Im}(Q(\kappa_{cx})) \end{Bmatrix} = 0 \quad (7)$$

with

$$[C(\kappa_{cx})] = \begin{bmatrix} [c_l] - \cos(\kappa_{cx})[c_r] & -\sin(\kappa_{cx})[c_r] \\ \sin(\kappa_{cx})[c_r] & [c_l] - \cos(\kappa_{cx})[c_r] \end{bmatrix}$$

2.3 Response in the frequency/wavenumber domain

For an external force $\{f\}$ applied to the system, s being the Laplace variable, the equations of motion take the frequency domain form

$$[Z(s)] \{Q(\kappa_{cx}, s)\} = \{F(\kappa_{cx}, s)\} \quad (8)$$

where the dynamic stiffness $Z(s) = Ms^2 + K$ contains mass, stiffness as well as hysteretic damping (constant imaginary part of K) or viscoelastic contributions (frequency and temperature dependent $K(s)$), see (Balmes 2013).

Each component of this Fourier series, that is to say each $\{Q_{\kappa_{cx}}\}$ for all $\kappa_{cx} \in [0, 2\pi]$ is then totally described by the system composed of the condition of continuity numbered 7 and by the following equation:

$$\begin{bmatrix} Z(s) & 0 \\ 0 & Z(s) \end{bmatrix} \begin{Bmatrix} \text{Re}(\{Q(\kappa_{cx}, s)\}) \\ \text{Im}(\{Q(\kappa_{cx}, s)\}) \end{Bmatrix} = \begin{Bmatrix} \text{Re}(F(\kappa_{cx}, s)) \\ \text{Im}(F(\kappa_{cx}, s)) \end{Bmatrix} \quad (9)$$

Accounting for continuity is done by elimination. One first seeks a basis T of $\ker([C(\kappa_{cx})])$ and uses it to solve the forced response

$$(T^T Z(s) T) Q = T^T F(s) \quad (10)$$

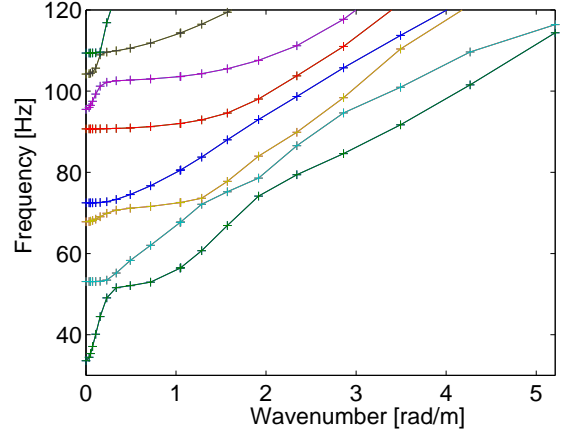


Figure 1: Choice of κ based on dispersion diagram

Computing this response at every target frequency $s = i\omega$ can be fairly long, modal synthesis methods are thus used. One first computes the periodic modes solutions of

$$(T^T [K - \omega_j^2 M] T) \{\phi_j\} = 0 \quad (11)$$

First order correction for the imaginary part of the dynamic stiffness is then used to obtain a reduced model for which the frequency response can be computed efficiently.

The second interest of computing periodic modes is to build a dispersion diagram showing the evolution of modal frequencies as a function of wavenumber. This motivates a strategy for choosing wave numbers. Instead of taking values evenly distributed in $[0, 2\pi]$ interval (which is the classic approach of discrete Fourier transform), the choice is made to refine the interval for small values of κ , and then to space the values as κ increases. This choice is justified looking at the shape of the dispersion diagram in Figure 1 which shows this diagram for a basic system composed of superstructure (rail modeled as a beam, pads, monoblock sleepers) only laying on 75 cm of ballast.

3 APPLICATION

3.1 Definition of track receptance

A widespread way to get information on track behaviour in dynamics is to perform a receptance test. It consists in measuring rail displacement at the point of the rail where a hammer impact is performed. This test characterises the global behaviour of track for a range of frequencies and allows to identify the resonances of the structure: it characterises the structure sensitivity to vibrations (Man 2002).

Receptance function is the transfer function between the displacement of the rail and the force applied:

$$H_{uF}^2 = \frac{S_{uu}}{S_{FF}} \quad (12)$$

Where H_{uF} is the track receptance

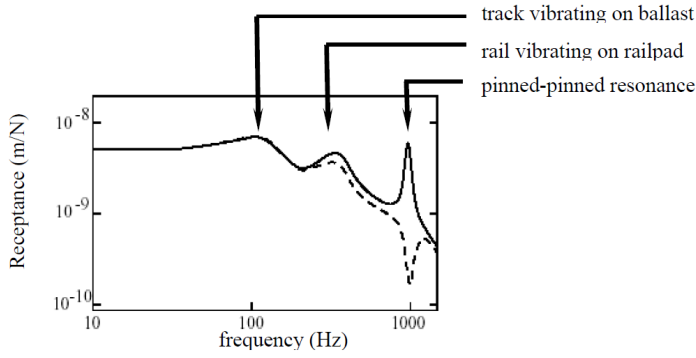


Figure 2: Typical receptance curve for ballasted tracks, from Dahlberg (2003)

Table 1: Frequency range in which the peaks of receptance curve can be found, (Knothe & Grassie 1993)

Point	Frequency range (Hz)
1	40-140
2	100-400
3	400-1200

S_{uu} autospectrum of displacement (in m^2s)

S_{FF} autospectrum of applied force (in N^2s).

For all ballasted tracks, receptance curve has the characteristic curve displayed in Figure 2 with three resonances. According to various authors (Knothe & Grassie 1993, Man 2002, Ferreira 2010, Ribeiro 2012), the first peak corresponds to full track resonant frequency, the second to baseplate resonant frequency and the last maximum is identified to pin-pin resonant frequency. All these points are related to vertical vibration modes of the track.

The frequency range in which these resonances can be found is summarised in Table 1.

Historically, receptance tests are used to calibrate material parameters in numerical or semi-analytical models (Knothe & Wu 1998). Superposition of the experimental curve with the one given by the model allows adjusting parameters.

The objective of the model validated here is to assess the track mechanical behaviour under a passing train. One thus focuses on the first part of the receptance curve (up to 150 Hz) and seek to see how this can be properly reproduced using a finite slice model of the track.

3.2 Comparison to 2.5D model

A receptance test has been modeled by Alves Costa et al. (2012), using a 2.5D FEM/BEM model, for the site of Carregado in Portugal.

This paragraph aims at comparing the results of

Table 2: Material properties

	Depth (m)	E (MPa)	ν	ρ (kg/m^3)	ξ
Ballast	0.22	97	0.12	1590	0.061
Subballast	0.35	212	0.20	1910	0.054
Embankment	0.30	212	0.20	1910	0.054
Soil	4	80	0.2	1900	0.06

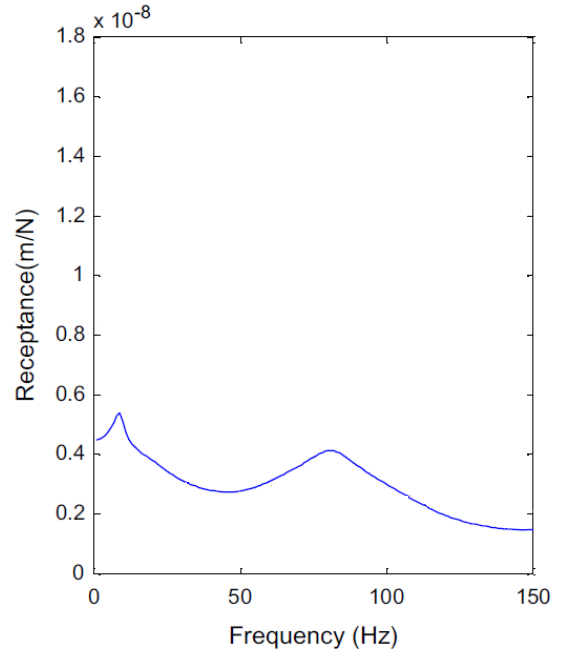


Figure 3: Receptance function for Carregado site, Alves Costa, Calçada, & A. Silva Cardoso (2012)

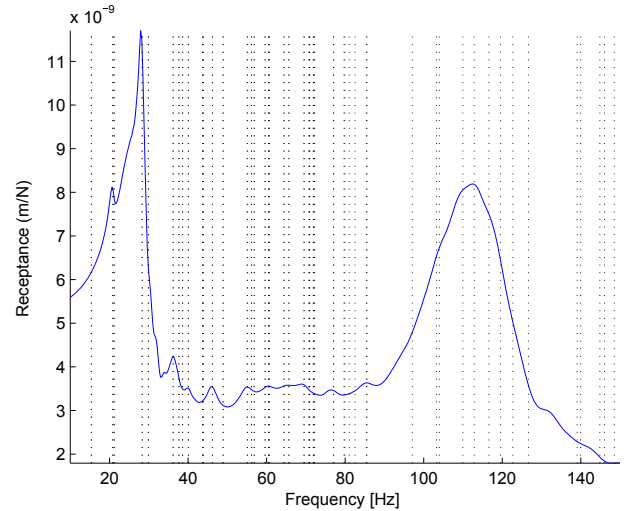


Figure 4: Computed receptance function for Carregado site

their work, displayed in Figure 3 to the receptance curve computed using the methodology described in part 2. The parameters used for the computation are summarised in Table 2. To get the result in Figure 4, equation 9 is solved for sixty values of κ , using a discretization of 0.2 Hz in frequency.

In Figure 3, only two resonance peaks can be identified, the first one at around 20 Hz and the second one at around 80 Hz. In the receptance curve computed in this work, these two peaks are clearly visible: the first one at 20 Hz, the second one at 110 Hz.

The main feature of the receptance in this frequency range is the global vertical track mode, first peak according to (Knothe & Grassie 1993) and both models agree on its frequency. The response shown for the 2.5D model seems much smoother and the levels differ. The origin of these differences is interesting to analyze. A probably critical source is the fact that the 2.5D FEM/BEM model considers infinite soil layers while the 3D periodic model presented in this pa-

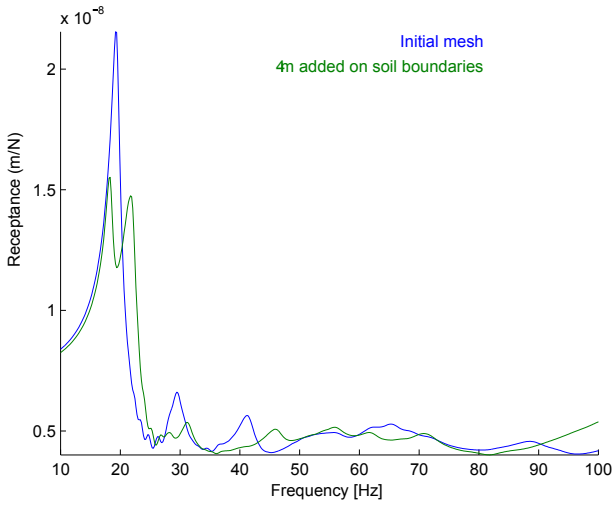


Figure 5: Comparison of receptance curve for a soil width of 6m (in blue) and of 10m (in green)

per considers a FEM slice which has a finite dimension. The choice of the width of soil to consider in a finite slice has a great influence on the receptance curve shape, as displayed in Figure 5. The level of the first resonance peak of the receptance curve decreases when the soil width taken into account increases which explains why the level of this peak in the FEM/BEM model is lower. A soil width of 10m will be used for the analysis below.

A second aspect is the fact that the 3D model allows a correct representation of sleepers and rail supports, which are assumed continuous in the 2.5D FEM/BEM model. Finally, the relatively coarse discretization in the wavenumber domain used here is another source of errors that needs to be investigated in relation with the cost of computing each wavelength.

3.3 Interpretation of the resonance peaks content

One of the main interests of the proposed approach is to offer a fine description of the receptance content. Beyond the correct reproduction of the response on the rail, a second step is to identify the mechanisms that generate the presence of resonances. Together with the forced response problem, the mode computations were performed using the same wavenumber (κ) distribution. The result can be represented using a dispersion diagram shown in Figure 6.

The peaks of the receptance curve in Figure 4 can be explained looking at this diagram: they all occur at a frequency corresponding to an horizontal part of a mode in the dispersion curve for small wavenumbers. For instance, the first peak at 18 Hz is principally linked to the second mode of the dispersion diagram, which is the first track compression mode. Table 3 shows the displacement of the track at the peaks of the receptance curve and the corresponding preponderant periodic mode (the modes displayed are materialised by a red cross in Figure 6). It is worth notice that the wider the horizontal part of a mode in the dispersion diagram is, the narrower the peak of the receptance curve is. Besides, the resonances identified

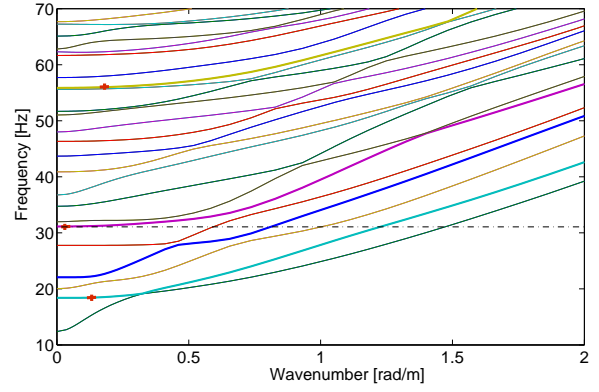


Figure 6: Dispersion diagram for Carregado site

Table 3: Forced response of track at the frequencies where peaks are found in receptance curve and corresponding modes for different values of κ

Forced Response	Periodic Mode
17.9 Hz	18.5 Hz, $\kappa=0.16$
31.3 Hz	31.1 Hz, $\kappa=0.03$
55.8 Hz	56 Hz, $\kappa=0.20$

in the receptance curve are the result of a combination of periodic modes as represented in Figure 6: at a given frequency, for instance 31 Hz, many periodic modes can be found intercepting the horizontal line for different wavenumbers.

There is no reciprocity, as not only eigen modes relative to vertical displacement of track are represented in the dispersion diagram. For instance, the first mode could have provoked a peak at 12.4 Hz, but as it is a shear mode as displayed in Figure 7, there is no impact of it on the receptance curve. On the contrary, all eigen modes affecting vertical displacement of track provoke or participate in creating a peak in the receptance curve. The different impact of modes in the receptance curve is also visible in Figure 4, in which the vertical dotted lines show the eigen modes for a given wavenumber κ (corresponding to a given length of track), in effect, many modes represented in this curve are not linked at all to any resonance peak.

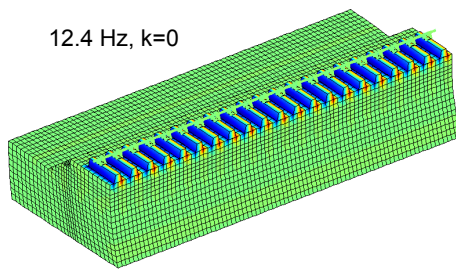


Figure 7: Periodic mode at 12.4 Hz corresponding to a wavenumber of 0

4 CONCLUSION

A methodology to compute track response in the frequency-wavenumber domain taking into account the 3D geometry of track have been proposed and compared to a 2.5D FEM/BEM model for the representation of a track testing: the receptance test. Some differences between the two results have been identified, but both models agree on the main characteristics of this test.

The present work deepens the understanding of the results of this widespread *in-situ* testing. The links between the periodic modes of the track and resonance peaks of the receptance test have been clarified. This relationship will be of great interest to compare track designs and to understand how to predict the track behaviour in dynamics.

Further steps will be the investigation of the need to extend the track model or to introduce absorbing boundary conditions to avoid the appearance of resonances associated with the finite nature of the slice. The validation of model reduction strategies that reconstruct the response based on computations for a few wavelengths and validations of strategies to build time domain damping models from the hysteretic models used here will be performed. Confrontation with experiments for both receptance and train passage will come next.

REFERENCES

- Alves Costa, P., R. Calçada, & A. Silva Cardoso (2012). Ballast mats for the reduction of railway traffic vibrations. Numerical study. *Soil Dynamics and Earthquake Engineering* 42, 137–150.
- Araújo, N. (2010). *High-Speed Trains on Ballasted Railway Track*. Ph. D. thesis, Universidade do Minho, Portugal.
- Balmes, E. (2004-2013). <http://www.sdtools.com/pdf/visc.pdf> Viscoelastic vibration toolbox, User Manual.
- Banimahd, M. & P. K. Woodward (2007). 3-dimensional Finite Element Modelling of Railway Transitions. In *Proceedings of Ninth International Conference on Railway Engineering, London*.
- Chebli, H., D. Clouteau, & L. Schmitt (2008). Dynamic response of high-speed ballasted railway tracks: 3D periodic model and in situ measurements. *Soil Dynamics and Earthquake Engineering* 28(2), 118 – 131.
- Connolly, D., G. Kouroussis, A. Giannopoulos, O. Verlinden, P. Woodward, & M. Forde (2014). Assessment of railway vibrations using an efficient scoping model. *Soil Dynamics*

- and *Earthquake Engineering* 58(0), 37 – 47.
- Dahlberg, T. (2003). *Railway track dynamics - a survey*. Technical report, Linköping University.
- Esveld, C. (1997). *Innovation in Railway Track*. TU Delft, –.
- Esveld, C. (2001). *Modern Railway Track, Second Edition*. MRT-Productions, Zaltbommel.
- Fernandes, V. A., F. Lopez-Caballero, & S. C. d’Aguiar (2014). Probabilistic analysis of numerical simulated railway track global stiffness. *Computers and Geotechnics* 55(0), 267 – 276.
- Ferreira, P. A. A. D. (2010). *Modelling and Prediction of the Dynamic Behaviour of Railway Infrastructures at Very High Speeds*. Phd, Universidade Técnica de Lisboa Instituto Superior Técnico.
- François, S., M. Schevenels, P. Galvín, G. Lombaert, & G. Degrande (2010). A 2.5D coupled FE/BE methodology for the dynamic interaction between longitudinally invariant structures and a layered halfspace. *Computer Methods in Applied Mechanics and Engineering* 199(2324), 1536 – 1548.
- Hall, L. (2003). Simulations and analysis of train-induced ground vibrations in finite element models. *Soil Dynamics and Earthquake Engineering* 23, 403–413.
- Knothe, K. & S. Grassie (1993). Modelling of Railway Track and Vehicle/Track Interaction at High Frequencies. *Vehicle System Dynamics* 22, 209–262.
- Knothe, K. & Y. Wu (1998). Receptance behaviour of railway track and subgrade. *Archive of Applied Mechanics* 68(7-8), 457–470.
- Kouroussis, G., O. Verlinden, & C. Conti (2011). Free field vibrations caused by high-speed lines: Measurement and time domain simulation. *Soil Dynamics and Earthquake Engineering* 31(4), 692 – 707.
- Krylov, V. V. (1995). Generation of ground vibrations by super-fast trains. *Applied Acoustics* 44(2), 149 – 164.
- Man, A. P. D. (2002). *Dynatrack: A survey of dynamic railway track properties and their quality*. Phd, Delft University.
- Ribeiro, A. C. C. A. (2012). *Transições aterra - Estrutura em linhas ferroviárias em alta velocidade: Análise experimental e numérica*. Phd, FEUP.
- Sternchüss, A. (2009). *Multi-level parametric reduced models of rotating bladed disk assemblies*. Phd, Ecole Centrale Paris.
- Yang, Y., H. Hung, & D. Chang (2003). Train-induced wave propagation in layered soils using finite/infinite element simulation. *Soil Dynamics and Earthquake Engineering* 23(4), 263 – 278.